Sjournals
Scientific Journals
Scientific Journal of Pure and Applied Sciences (2012) 1(3) 144-161
ISSN 2322-2956

Contents lists available at Sjournals
Scientific Journal of
Pure and Applied Sciences
Journal homepage: www.Sjournals.com

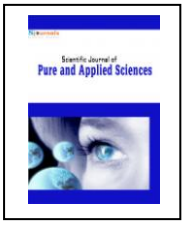

Original article

Application of piezoceramic transducers for 3D Impedance modelling in damage assessment of plate

M.A. Radhika[a], V.G.M. Annamdas[a,*], Y. Yang[b]

[a]*Laboratory of Monitoring Science, Nanyang Technological University, 50 Nanyang Avenue, Singapore 639798.*
[b]*School of Civil and Environmental Engineering , Nanyang Technological University, 50 Nanyang Avenue, Singapore 639798.*

[*]Corresponding author: Venu Gopal M. Annamdas (annamdas@ntu.edu.sg), Founder and Coordinator, Laboratory of Monitoring Science.

ARTICLE INFO

Article history:
Received 24 November 2012
Accepted 19 December 2012
Available online 28 December 2012

Keywords:
PZT
Plates
Damage
Propagation
Frequency proximity index (FPI)
Non-destructive evaluation (NDE)
Structural health monitoring (SHM)

ABSTRACT

Cost-effective and reliable damage detection models are crucial for successful monitoring of any ancient or modern age engineering structure. Piezoceramic transducers (PZT) based electromechanical impedance (EMI) method is emerging as a promising alternate for conventional structural health monitoring (SHM) of various structures. The PZTs are usually surface bonded and then excited in the presence of electric field to a desired frequency range. The excitations result in prediction of unique frequency dependent electromechanical (EM) admittance signature. Any change in the signature during the monitoring period indicates dis-integrity in the structure. However, apart from locating damages, the increase in severity has to be predicted on time to avoid collapse of the entire structure. This paper presents such a model which had effectively predicted the severity of damages along two principle directions. This was achieved by experimental damage study on plates and subsequent verification by semi numerical 3D model. Statistical root mean square deviation (RMSD) index was used for evaluating the damages made on plates. A new frequency proximity index (FPI) was also introduced to measure the effectiveness of the model. RMSD measures the changes in height of peaks of signature and FPI scales the frequency spectrum of signature. Thus results of RMSD index and FPI are used as complementary to each other to study damage propagation in a structure.

1. Introduction

Piezoceramic transducers (PZT) based electromechanical impedance (EMI) method is emerging as a promising alternate for conventional structural health monitoring (SHM) of various engineering structures (Annamdas and Soh, 2010). These PZT transducers are small size smart materials which can be used in single PZT or multiple PZT (Annamdas and Soh, 2008) structure interaction models. Especially in the last decade, EMI based SHM technique has been successfully applied to aerospace and aircraft structures (Chaudhry, et al., 1995; Giurgiutiu, et al., 2001; Ghoshal, et al., 2001; Xu, et al., 2004), and civil structures (Ayres, et al., 1998; Park, et al., 2001; Park, et al., 2005; Yang, et al., 2008; Annamdas and Yang, 2012; Annamdas, 2012). In the EMI technique, the PZT transducers are generally surface bonded to the host structure and subjected to electrical excitation over the desired frequency range. This results in the electromechanical (EM) admittance (inverse of impedance) signature of the PZT transducer. Due to the EM coupling effect between the PZT and the structure, any change in the EM admittance signature could be indicative of the presence of structural damages (Sun, et al., 1995). However, apart from locating damages, the increase in severity of damages has to be predicted on time to avoid collapse of the entire structure. This paper presents such a model which had effectively predicted the severity of damages along X and Y directions of the structure. This was achieved by experimental damage study on plates and subsequent verification of semi numerical three dimensional (3D) model (Annamdas and Soh, 2007a,b) by employing a new frequency proximity index (FPI). Statistical root mean square deviation (RMSD) index was used for evaluating the damages made on plates. Thus, results of RMSD index and FPI are used as complementary to each other to study damage propagation in a structure.

First, an experimental damage study was carried out on two identical plates. For this purpose, holes were drilled on the plates along X and Y directions, each drilled hole represented new damaged state of plate. EM admittance signatures were recorded over a frequency spectrum at each damaged state. Next, numerical simulations using finite element analysis (FEA) was carried out for all the damaged states and the 3D EMI model is applied to calculate the PZT EM admittance. The damage was quantified by the RMSD index and FPI. The correlation of the RMSD index with the location of damage and the distance from PZT was also investigated.

2. Materials and methods

2.1. Experimental admittance signatures

As shown in Figure 1, the experimental setup consisting of an HP 4192A impedance analyzer (Hewlett Packard, 1996) a 3499A/B switching box (Agilent Technologies, 2007) and a PC was used to acquire the PZT admittance signatures. The PZT patch was wired to the impedance analyzer through the switch box with a sinusoidal 1-volt electrical supply (E_3) resulting in actuations. The EM admittance signature was acquired over the desired frequency spectrum.

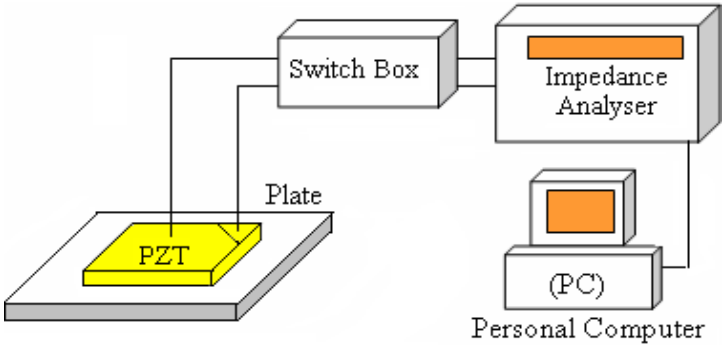

Fig. 1. Experimental setup

Park et al. (2003) recommended that the frequency spectrum should be kept less than 500 kHz to ensure high sensitivity to incipient damage. They further recommended that frequency larger than 500 kHz is unfavourable because the sensing region becomes extremely localized and the PZT patch shows adverse sensitivity to their bonding conditions. At extremely high frequency, the sensing range becomes very limited and the resonance of the PZT patch dominates that of the structure, thus rendering the outcome of sensing ambiguous and inefficient. Hence in the present study a frequency spectrum up to 500 KHz was considered first and later it was narrowed down (see later sections) to obtain more stable spectrum which predicts consistent trends with increase in damage severity. Additionally, the EM admittance signature is a complex term, which can be separated into real and imaginary parts. However, only the real part (Sun, et al., 1995) of EM admittance represents active interaction with the structure as compared to the imaginary part, hence in the present study only real admittance was used for comparisons.

2.2. Experimental specimens

As shown in Figure 2, two aluminum (of grade A1 6061-T6) plate specimens (Table 1) designated as X and Y of the same size were used as the host structures to be monitored. Two identical PZT patches (PI Ceramic, 2007), one each on plate X and Y was surface bonded at the centre using a thin layer of high strength epoxy adhesive (RS Components, 2007). The dimensions and properties of the plate specimens, PZT and epoxy adhesive are summarized in Tables 1-2.

Table 1
Dimensions of plates, PZT patches and damage holes.

Plate / Patch / damage /spacing	Dimensions
X / Y	150 x 300 x 2 mm^3
PZT	10 x 10 x 0.3 mm^3
Hole	5 mm diameter
Spacing between 2 holes	10 mm

Figure 2(a) shows damages induced on plate X along direction X by drilling 6 small holes sequentially with a space of 10 mm. The first hole was drilled at a distance of 15 mm and the last (the sixth) hole at 65 mm from the PZT. Each new hole drilled represented a new damage state of the specimen. And each damaged state (designated as X1, X2, … X6) was assessed by acquiring the admittance signatures of the PZT, and comparing them with the signature acquired for the undamaged or baseline state (designated as X0). Similarly as shown in Figure 2(b), five damaged states were induced on plate Y (designated as Y1, Y2, … Y5) along direction Y and six admittance signatures including the undamaged state (designated as Y0) signature were recorded and compared.

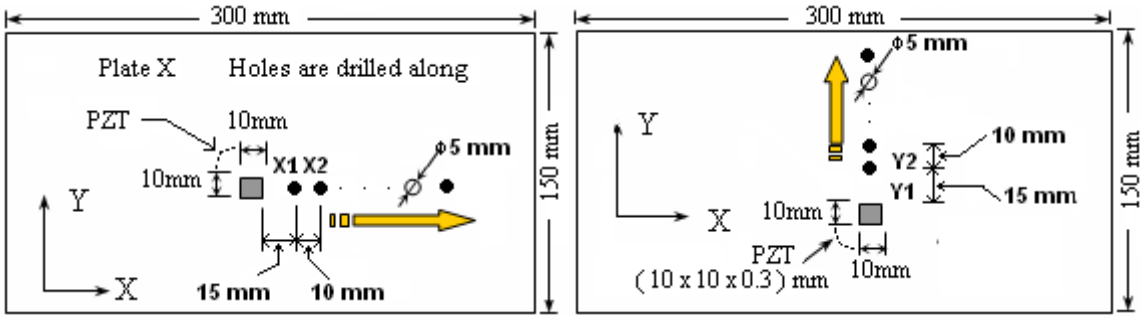

(a) (b)

Fig.2. Damage propagation on plates (a) X (b) Y

Table 2
Key properties of epoxy adhesive (RS 850-940), plate and PZT

Physical property	Value		
	Epoxy	Plate	PZT
Mechanical			
Density (kg/m^3)	1180	2715	7800
Young's Modulus (N/m^2) x 10^9	2	68.95	66.67
Poisson ratio	0.4	0.33	0.33
loss factor, η	-	-	0.023
Dynamical			
Mass damping factor α		0	
Stiffness damping factor β x10^{-7}		1.5923	
Electrical			
Piezoelectric strain coefficients (m/V) d_{31} , d_{32} x 10^{-10}			-2.10
Piezoelectric strain coefficient (m/V) d_{33} x10^{-10}			4.50
Dielectric loss factor, δ			0.015
Electric permittivity, ε_{33} (farad/m) x 10^{-8}			1.75

2.3. Predicted admittance signatures: overview of 3D impedance model

In the EMI technique, modeling of PZT-structure interaction is essential for damage assessment of the structures. In the last decade, various EMI models (Liang, et al., 1996; Zhou, et al., 1996; Yang, et al., 2005; Annamdas, et al., 2007; Hu and Yang, 2007) have been proposed using this EMI technique. The directional sum impedance (DSI) model developed by Annamdas and Soh (2007a) is used in the present study as it examines the 3D interaction between the PZT and the host structure.

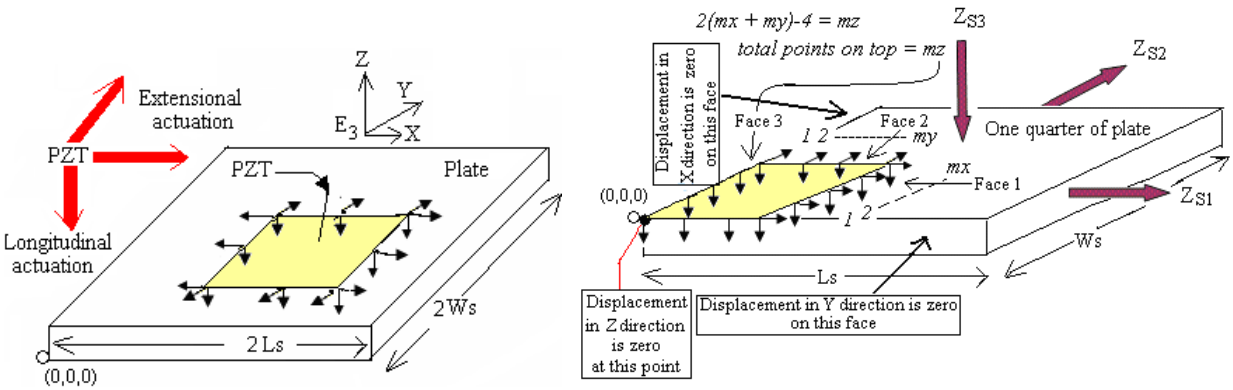

Fig.3. Unsymmetrical and symmetrical plates with surface bonded PZT transducer
(a) Actuations of PZT in presence of electric field E_3
(b) Linear impedances with unit distributed forces for one quarter of plate

In general, the actuation mechanism of the PZT patches in the presence of electric field along the Z direction (Figure 3) can be divided into extensional (along the X and Y directions) and longitudinal (along Z direction) actuations. While the previous models considered only extensional actuation, the 3D DSI model took into account both the extensional and longitudinal actuations. The formulations are presented as follows, Figure 3(a) shows a

PZT patch with length 2L, width 2W, and thickness 2H, is bonded at the centre of a plate with length 2Ls, width 2Ws and thickness 2Hs, and with unsymmetrical boundary conditions along the X and Y directions of the plate. EM admittance of PZT for such a geometrically unsymmetrical plate can be expressed as

$$\overline{Y_A} = \frac{j\omega(2L)(2W)}{2H}\left\{\bar{\varepsilon}_{33} + Y_R(d_{31}\lambda_1\left\{\begin{matrix}[A_0\sin kL - d_{31}] \\ + R[C_0\sin kW - d_{32}] + R[E_0 k\cos k2H - d_{33}]\end{matrix}\right\}\right.$$

$$+ d_{32}\lambda_2\{R[A_0\sin kL - d_{31}] + [C_0\sin kW - d_{32}] + R[E_0 k\cos k2H - d_{33}]\}$$

$$\left. + d_{33}\lambda_3\{R[A_0\sin kL - d_{31}] + R[C_0\sin kW - d_{32}] + [E_0 k\cos k2H - d_{33}]\})\ \right\} \quad (1)$$

However, for a plate with symmetrical boundary conditions along X and Y directions as shown in Figure 3(b), only one-quarter has to be considered. i.e replace 2L and 2W by L and W respectively in Equation (1) to obtain admittance of one-quarter plate. Later, to get admittance for complete plate, the obtained one-quarter admittance has to be multiplied by 4.

where ω and *k* are the angular frequency and wave number respectively, and their relationship is given as

$$k = \omega\sqrt{\frac{\rho(1+\nu)(1-2\nu)}{\overline{Y}(1-\nu)}} \quad (2a)$$

$\overline{\varepsilon_{33}}$ is the complex electric permittivity of the PZT at zero stress, expressed as

$$\overline{\varepsilon_{33}} = \varepsilon_{33}(1-\delta j) \quad (2b)$$

The electric field E_3 along Z direction is given as

$$E_3 = \frac{V}{2H} \quad (2c)$$

Where *V* is voltage constant, δ is the dielectric loss factor and ε_{33} is the static electric permittivity of the PZT patch d_{3p} is the strain displacement coefficient related to the normal strains in the presence of electric field, and the subscript *p*(=1,2,3) denotes the X, Y and Z directions. *R* and Y_R are the simplification parameters, given as

$$R = \frac{\nu}{1-\nu}\ ,\ Y_R = \overline{Y}\ \frac{1-\nu}{(1+\nu)(1-2\nu)} \quad (3)$$

where ν is the poison's ratio and $\overline{Y}$ is the complex Young's modulus of the PZT patch at zero electric field, expressed as

$$\overline{Y} = Y(1+\eta j) \quad (4)$$

where Y is the static Young's modulus and η is the mechanical loss factor. λ_1, λ_2 and λ_3 are the response factors along the X, Y and Z directions, given as

$$\lambda_1 = \left(\frac{Z_{S1}}{Z_{S1} + Z_{S2} - Z_{S3}} \right),\ \lambda_2 = \left(\frac{Z_{S2}}{Z_{S1} + Z_{S2} - Z_{S3}} \right) \text{ and } \lambda_3 = \left(\frac{Z_{S3}}{Z_{S1} + Z_{S2} - Z_{S3}} \right) \quad (5)$$

where Z_{S1}, Z_{S2} and Z_{S3} are the linear impedances of the plate along the X, Y and Z directions, respectively. The 3D model is semi analytical in nature since Equation (1) comprises of some parameters (λ_1, λ_2, λ_3, A_0, C_0, E_0) that need to be determined by FEA. However, to solve these parameters, linear impedances in Equation (5) need to be defined first.

Z_{S1} is the ratio of sum of the distributed load to the sum of velocities produced at the points of consideration, written as

$$Z_{S1} = \frac{\sum_{1}^{mx} F_1}{\sum_{i=1}^{mx} \dot{u}_i} = \frac{F_X}{\dot{u}_1} = \frac{F_X}{j\omega u_1} \quad (6)$$

where F_1 = 1+0*j* is the distributed force applied on the host structure on edges of the PZT patch on face 1, as shown in Figure 3; *mx* is the number of points considered on face 1; $\dot{u}_i$ is the velocity of the i^{th} point in direction X; F_X is the sum of distributed harmonic load of all the considered points along X direction. Z_{S2} and Z_{S3} are defined as similar to that given by Annamdas and Soh (2007a).

The coefficients A_0, C_0 and E_0 are defined as

$$A_0 = \frac{a_4 - a_2 c_0 - a_3 E_0}{a_1}, \qquad C_0 = \frac{(b_4 c_1 - b_1 c_4) - (b_3 c_1 - b_1 c_3) E_0}{(b_2 c_1 - b_1 c_2)}$$
$$E_0 = \frac{(a_4 b_1 - a_1 b_4)(b_2 c_1 - b_1 c_2) - (a_2 b_1 - a_1 b_2)(b_4 c_1 - b_1 c_4)}{(a_3 b_1 - a_1 b_3)(b_2 c_1 - b_1 c_2) - (a_2 b_1 - a_1 b_2)(b_3 c_1 - b_1 c_3)} \quad (7)$$

where

$$a_1 = (R_1\ L\cos kL - Z_{S1}\ j\omega L \sin kL),\ a_2 = (R\ R_1\ W\cos kW),$$
$$a_3 = (R\ R_1\ \cos 2kH),\ a_4 = R_1\,(d_{31} + R(d_{32} + d_{33}))$$
$$b_1 = (R\ R_2\ L\cos kL),\ b_2 = (R_2\ W\cos kW - Z_{S2}\ j\omega W \sin kW)$$
$$b_3 = (R\ R_2\ \cos 2kH),\ b_4 = R_2\,(d_{32} + R(d_{31} + d_{33}))$$
$$c_1 = (R\ R_3\ W\cos kW),\ c_2 = (R\ R_3\ L\cos kL),$$
$$c_3 = (R_3\ \cos 2kH - Z_{S3}\ j\omega \sin 2kH),\ c_4 = R_3\,(d_{33} + R(d_{31} + d_{32}))$$
$$R_1 = 2kWH,\ R_2 = 2kLH,\ R_3 = kLW$$

All the parameters in Equation (1), can be determined obtained using FEA. More details of derivation of the above formulae are presented in Annamdas and Soh (2007a,b).

2.4. Boundary conditions

Free-free boundary condition was assumed for all damaged states of plates X and Y (resting freely on foam). At the undamaged state, the specimens were symmetric along both X and Y directions (Figure 4a). Admittance signatures for the undamaged state were obtained by multiplying 4 to the one-quarter admittance i.e for X0, Y0 as explained previously.

$$Y_{Baseline} = 4\ \overline{Y_A} \quad (8)$$

where $Y_{Baseline}$ represents the admittance signature for baseline cases of complete X or Y plates. However, for other damaged cases the admittance is obtained by Equation 1 (see Figure 4b)

i.e., $$Y_{X1.....X6/Y1.....Y5} = \overline{Y_A} \quad (9)$$

where $Y_{X1.....X6/Y1.....Y5}$ represents admittance signature for damaged states of either plate X or Y.

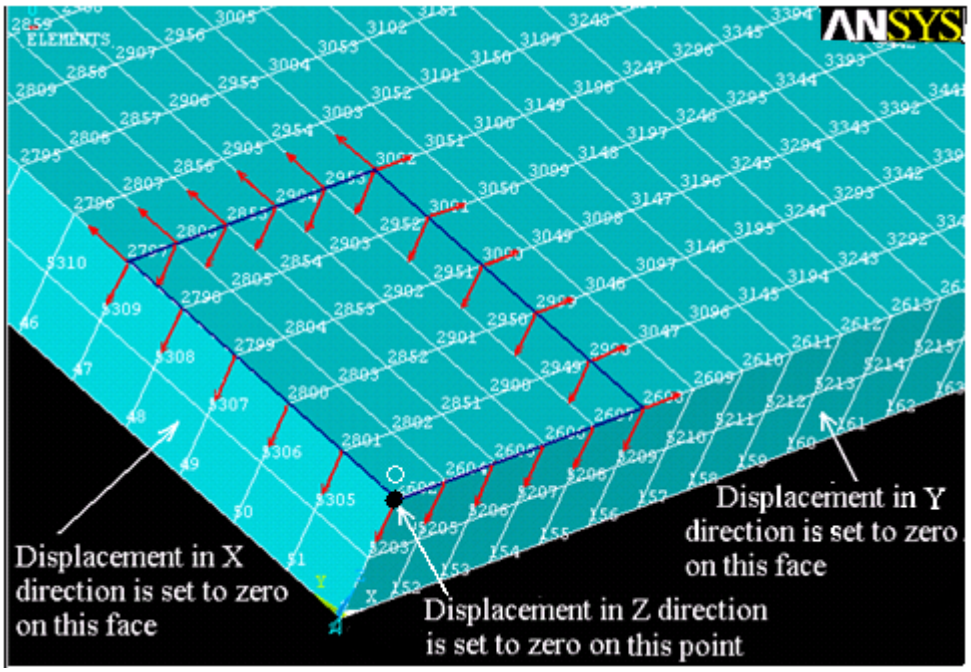

(a)

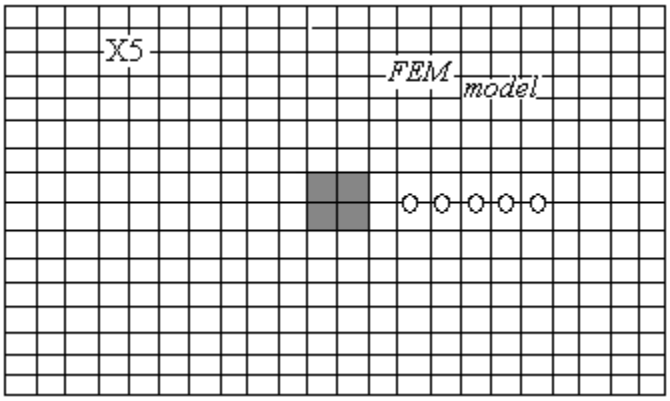

(b)

Fig.4. FE modelling of one quarter of specimen with unit distributed forces on central location of plate (a) FE model of one-quarter of plate X (b) plan of FE model for plate X

2.5. Finite element analysis

2.5.1. Baseline signatures

As previously explained, 3D predicted admittance signatures need a part of solution to be solved using numerical (FE) analysis (see Equation 5 and 6). The modelling for baselines of plates X and Y were performed for only one-quarter of the plate, i.e for half length and half width of plate as shown in Figure 4(a). The mesh sizes adopted are 1 mm x 1 mm x 1 mm for both the plates. Appropriate boundary conditions were imposed on the planes of symmetry, i.e, the X and Y components of the displacement were set to zero on the YZ and on the ZX planes of symmetry, respectively. In addition, at the centre of the PZT patch, the Z component of the displacement

was set to zero as shown in Figure 4(a). The FE meshing was carried out using ANSYS 5.6 (ANSYS, 2000). The quarter of plate was discretised into 3D brick elements (solid 45) possessing 3 degrees of freedom at each node. The assumption made was to use the unit distributed forces exerted by the quarter of PZT patch (full patch for unsymmetrical plate), i.e the unit harmonic forces were applied directly on the host structure along the edges of the equivalent one-quarter dimension of the patch in the three principle directions as shown in Figure 3 (also Figure 4). This is in accordance with the extensional and longitudinal actuations of the patches. The dynamic harmonic analysis was performed and the complex displacement responses at the points of force application were obtained over the frequency range of 0—100 kHz. As explained previously, the linear impedances are determined for the one-quarter plate as given below.

Z_{S1} was determined as a ratio of sum of the distributed load (i.e total force) to the sum of output velocities (i.e differentiation of displacement with respect to time) produced at the points/ nodes of consideration. i.e the output displacement response is substituted in Equation 6 to get linear impedance along X. Similarly, the linear impedances along directions Y and Z (ie, Z_{S2} and Z_{S3}) were determined using FE analysis. The other unknowns were determined as explained similar to that of Annamdas and Soh (2007a,b). Thus all the unknowns which were not determined using analytical equations were determined using FEA.

2.5.2. Damaged state signatures

Figure 4(b) shows a representative damaged state of plate X. The whole structure was modelled. Similar modelling was done for damages on Y direction for plate Y. The final admittance signature was obtained for all damaged states of plates X and Y using Equation 9.

3. Results and discussion

3.1. Frequency spectrum

A total of 13 (X0, X1…X6, Y0, Y1...Y5) 'real' admittance signatures for a broader excitation frequency spectrum of 0-500 kHz and higher resulted in lateral and vertical shifts in predominant peaks of real admittance signatures. Moreover, the directions of shifts were not consistent due to localising effect (Park et al 2003). Similar inconsistent peaks shifts were also observed in imaginary admittance signatures and it is difficult to comment on changes in the signatures by observing the raw data of all damage states. However for smaller frequency spectrums (say 0 to 50 kHz or 0-100 kHz) the trends were more consistent. Figures 5 (a-b) and Figure 6 (a-b) show the experimental real admittance signatures for plates X and Y. Figures 5 (c-d) and Figures 6 (c-d) show the predicted real admittance signatures. For the considered frequency spectrum there exists satisfactory matching of experimental and predicted signatures.

3.2. Comparisons and discussions

Figures 5 (c) and 6 (c) show that the frequency spectrum of 0-50kHz, which yielded slightly taller peaks in 3D predicted model as compared to experimental admittance signatures. However from the pattern of figures by our naked eye, (Figures 5b and 6b) we observe that the frequency spectrum of 0-100 kHz yielded much similar peaks as compared to experimental admittance signatures for all damage cases. The quantitative measure of damage was done using RMSD, which uses change in signature peaks/ valleys of baseline and subsequent damaged state to quantify the damage. The RMSD index comparisons are given in Figure 7. The trend lines for experimental and predicted signatures show increase in magnitude with increase in damage severity for both plates X and Y for the considered frequency range of 0-50 kHz. This was further verified for frequency range of 0-100 kHz as shown in Figures 5(b-d) and Figures 6(b-d).

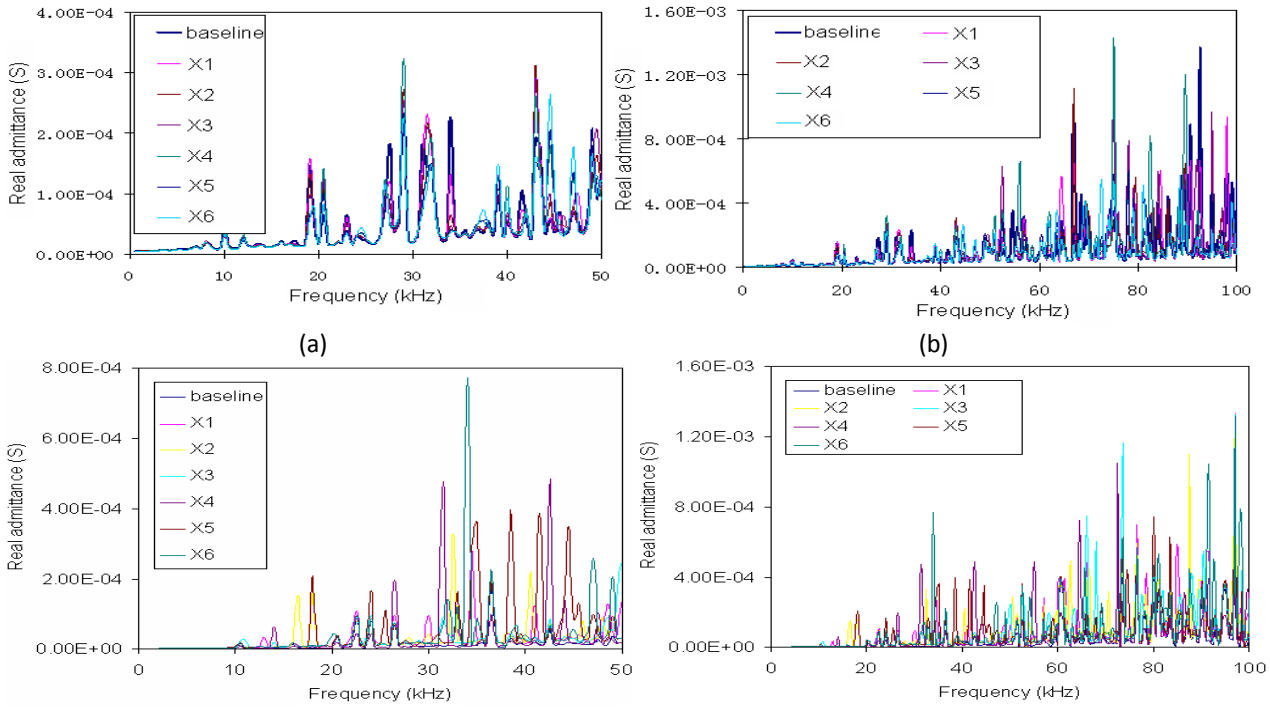

Fig.5. Real admittances for frequency spectrum 0-50 kHz and 0-100 kHz for plate X
(a) Experimental signature for 0-50 kHz (b) Experimental signature for 0-100 kHz (c) Predicted signature for 0-50 kHz (d) Predicted signature for 0-100 kHz

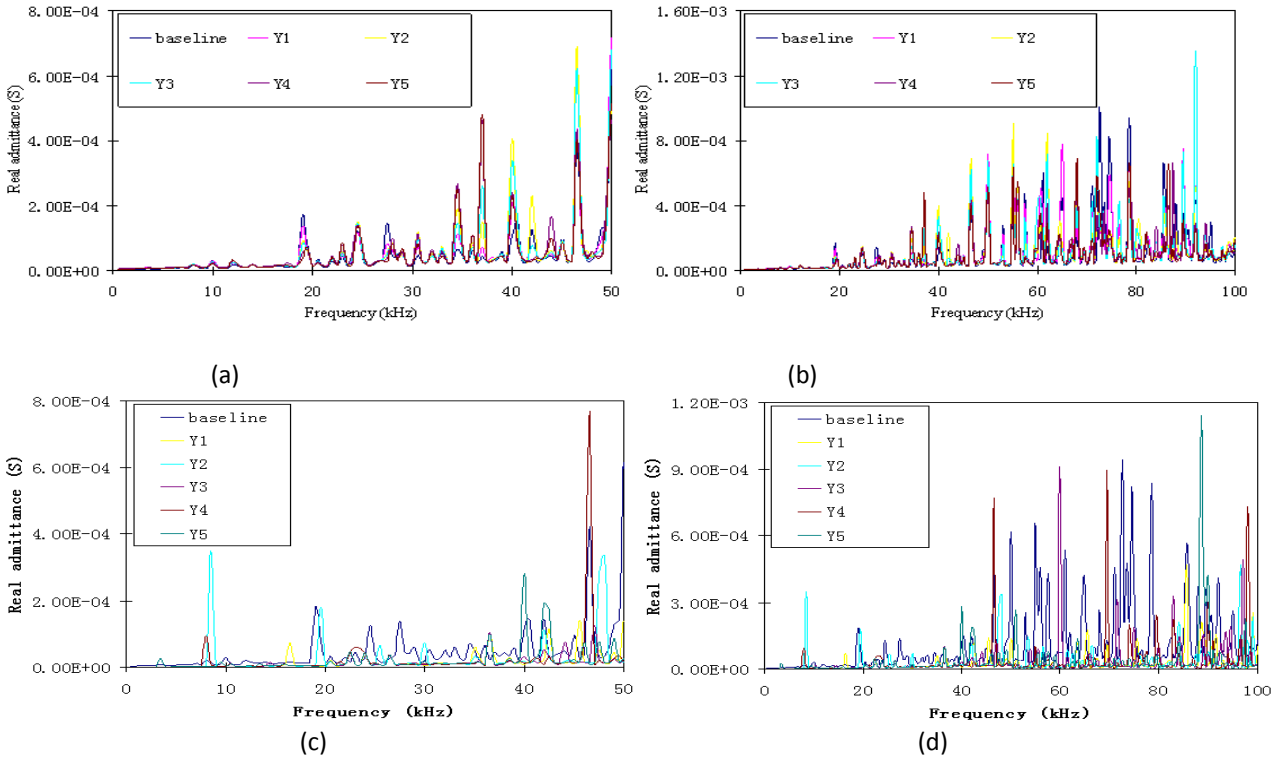

Fig.6. Real admittances for frequency spectrum 0-50 kHz and 0-100 kHz for plate Y
(a)Experimental signature for 0-50 kHz (b) Experimental signature for 0-100 kHz
(c) Predicted signature for 0-50 kHz (d) Predicted signature for 0-100 kHz

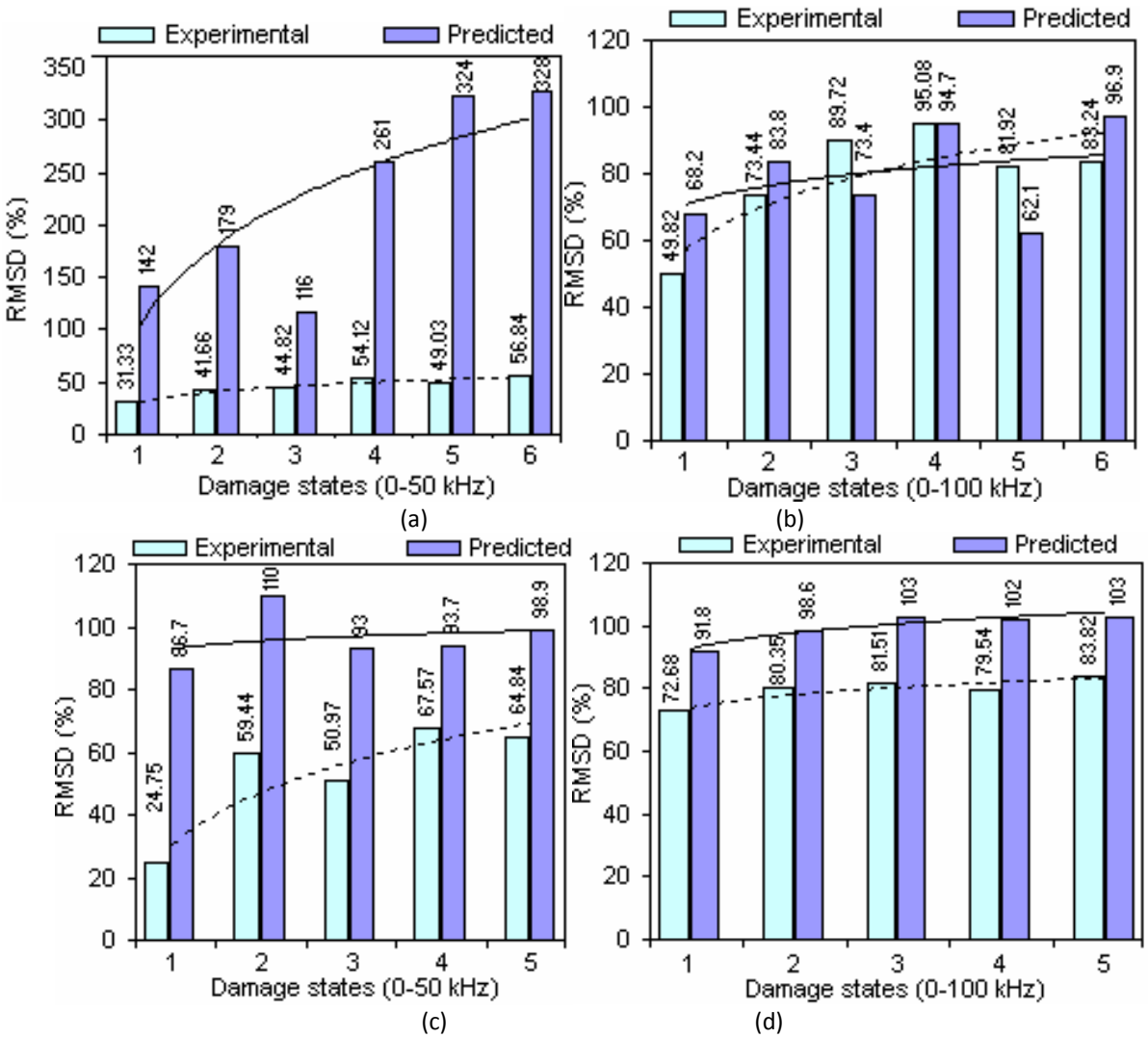

Fig.7. RMSD for various damaged cases in two frequency spectrums
(a)For plate X in 0-50 kHz (b) For plate X in 0-100 kHz
(c) For plate Y in 0-50 kHz (d) For plate Y in 0-100 kHz

Figures 5 to 7 shows that the 3D predicted model was successful to model PZT-structure interaction. However, pattern recognition of signatures or RMSD index do not reveal the proximity of any predicted model to experimental model. This is because, the pattern recognition of signature employs our naked eye and RMSD employs only peak / valley shifts to quantify ignoring frequency spectrum of excitation (Annamdas and Soh 2007a). Tables 3 and 4 lists respectively both the experimental and predicted peak frequency locations for baseline and damaged states of plates X for frequency range between 10-100 kHz (high frequency spectrum).

In any EM admittance signature peaks or valleys occurring in the considered spectrum either for low frequency (say upto 10 kHz , Yang et al 2005) or high frequency (say 10 -100 kHz, Annamdas and Soh 2007b) are important. Observations revealed that the first major peak in experimental and predicted occurred at 10 kHz and 10.5 kHz respectively. There were some splitting and merging of peaks as damage propagated along X direction in both experimental and predicted signatures. For example, Figure 8 shows the characterization of peaks, i.e Figure 8(a) shows splitting of peak (of X1) due to second damage (X2).

Table 3
Experimental peak frequency (kHz) occurrence for plate X.

X0	X1	X2	X3	X4	X5	X6
10	10	10	10	10	10	10
12	12	12	12	12	12	12
16	16	16.5	16	14	16	14
20.5	17	19	20.5	16	19.5	16
23	19	20.5	22.5	17	20.5	17
24	20.5	23	24	20.5	23	20.5
35.5	22	24.5	27	23	24.5	23
37	24	27	29	24.5	27	24.5
39	27.5	29	32	27	29.5	27
40	29	31.5	36.5	29	32	29
41.5	31.5	34	39	32	34.5	32
44.5	34	37	40	35.5	35.5	37.5
47	35.5	39	43	37.5	39	39
49	37	40	46	39	40	40
51	38	42	47	41	42	42
52	39	44.5	49.5	42	43.5	44.5
54.5	41.5	47	51	44.5	44.5	47
57	43	49.5	52.5	47	47	49
58.5	44.5	51	57	49.5	49	50
60.5	45.5	52.5	58.5	51	50	51
62	47.5	54	59.5	52.5	51	52.5
63.5	49	55.5	60.5	56	52	54
64.5	50	57	63.5	57.5	54	55.5
67	51	58.5	65	58.5	55.5	58.5
69.5	52	60	66	60.5	57	60.5
74	55.5	62	67	62	58.5	62
75	57	65	68	63.5	60.5	63.5
76.5	58.5	67	69	65	62	64.5
78	60.5	69.5	71.5	68	63.5	67
79	63.5	71.5	74	69.5	64.5	68
81	64.5	72.5	74.5	71.5	67	69
82.5	67	74	76	72.5	68	70.5
84	69.5	76	78	74	69	71.5
86	71.5	78	79.5	75	71.5	72.5
88	74	79.5	81.5	76.5	72.5	75
90.5	75.5	81	87	78	74.5	76.5
91.5	78	83	88	79	76.5	78
92.5	79.5	84	89.5	81	78	80
95	81	87	90.5	82.5	80	81
98	82.5	88.5	92	86	84	82.5
99	84.5	89.5	95	89.5	85	86.5
	87	90.5	97	92	86.5	88.5
	89.5	91.5	98	95	88.5	89.5
	90.5	94		96.5	89.5	92
	91.5	95		99.5	90.5	95
	92.5	97			92	97
	95	98			95	99
	96.5				97	
	98				99.5	
	99					

Table 4
Predicted peak frequency (kHz) occurrence for plate X.

X0	X1	X2	X3	X4	X5	X6
10.5	10.5	10.5	11	10.5	10.5	10.5
12.5	13	12.5	12.5	12.5	12.5	12.5
16	16	16.5	16	14	16	15
20.5	18	18	20.5	16	19	16
22.5	19.5	20.5	22.5	18	20.5	17
24	20.5	22.5	24	20.5	22.5	20.5
35.5	22.5	24	26.5	22.5	24	22.5
36.5	24	26.5	29	24	26.5	24
38.5	26.5	28	31.5	26.5	28	26.5
39.5	30	32.5	36.5	28.5	31	29
41	33	34	38.5	31.5	35	32
44.5	34.5	36.5	40.5	35.5	36.5	37.5
47.5	35.5	38.5	42.5	36.5	38.5	39
49	36.5	39.5	46	38.5	39.5	40
51.5	38.5	42.5	47	41	41.5	42.5
52.5	39.5	44.5	50	42.5	42.5	45
54	41	47	51.5	44	44.5	47
57	42.5	49	52.5	47.5	47	49
59.5	44.5	50.5	57	48.5	49	50
61	45.5	52.5	58	51.5	50.5	51.5
62	47.5	54	59.5	52.5	51.5	52.5
63	48.5	55	60.5	55	52.5	54
64	50	57	63.5	57	53.5	56
66	51.5	59.5	64.5	58	56	58
69.5	52.5	60.5	66	60.5	57	60.5
73.5	55	62.5	67	62	58	62
74.5	57	64.5	68	63	60.5	63
76.5	58.5	66.5	69	64.5	62	64..5
78	60.5	69.5	72	68	63	67
80	63	71.5	73.5	69.5	64	68
81	64	72.5	75	71.5	66	69
82	67	73.5	76.5	72.5	68	70.5
83.5	69.5	76.5	77.5	73.5	69	71.5
85.5	71.5	78.5	80	75	72	73.5
87	73.5	80	81	76.5	73.5	75
90	75	81	87	78	74.5	76.5
91.5	78.5	83.5	88	80	76.5	78
93	80	85	89.5	81	78	80
95	81	87.5	90.5	82.5	80	81
97	82	88.5	93	87	83.5	82.5
98.5	85	90	95	90	85.5	85.5
	87	91	97	91.5	87	87.5
	88.5	92	98.5	95	88.5	90
	90	93		97	90	92.5
	91.5	95		99.5	91	95
	93	97			93	97
	95	98.5			95	98
	97				97	
	98.5				98.5	
	99.5					

Figure 8(b) shows peak (of X2) emerging and vanishing due to third damage (X3). Similarly, Figure 8(c-d) shows the splitting, emerging and vanishing of peaks in predicted signatures. This is similar to that of splitting and

merging of PZT signature peaks observed by Annamdas et al (2007) for load increments on the structure. Additionally, number of peaks changed with damaged states in both experimental and predicted signatures. Thus, this present study lead to an idea of using occurrence of peak i.e peak frequency, number of peak matches, closeness and farness of peaks in a given frequency spectrum. This is to study the proximity of experimental and predicted admittance signatures. This is named as Frequency Proximity Index (FPI) and can serve as complementary to RMSD and pattern recognition methods. i.e RMSD measures the changes in height of peaks of signature and FPI scales the frequency spectrum of signature.

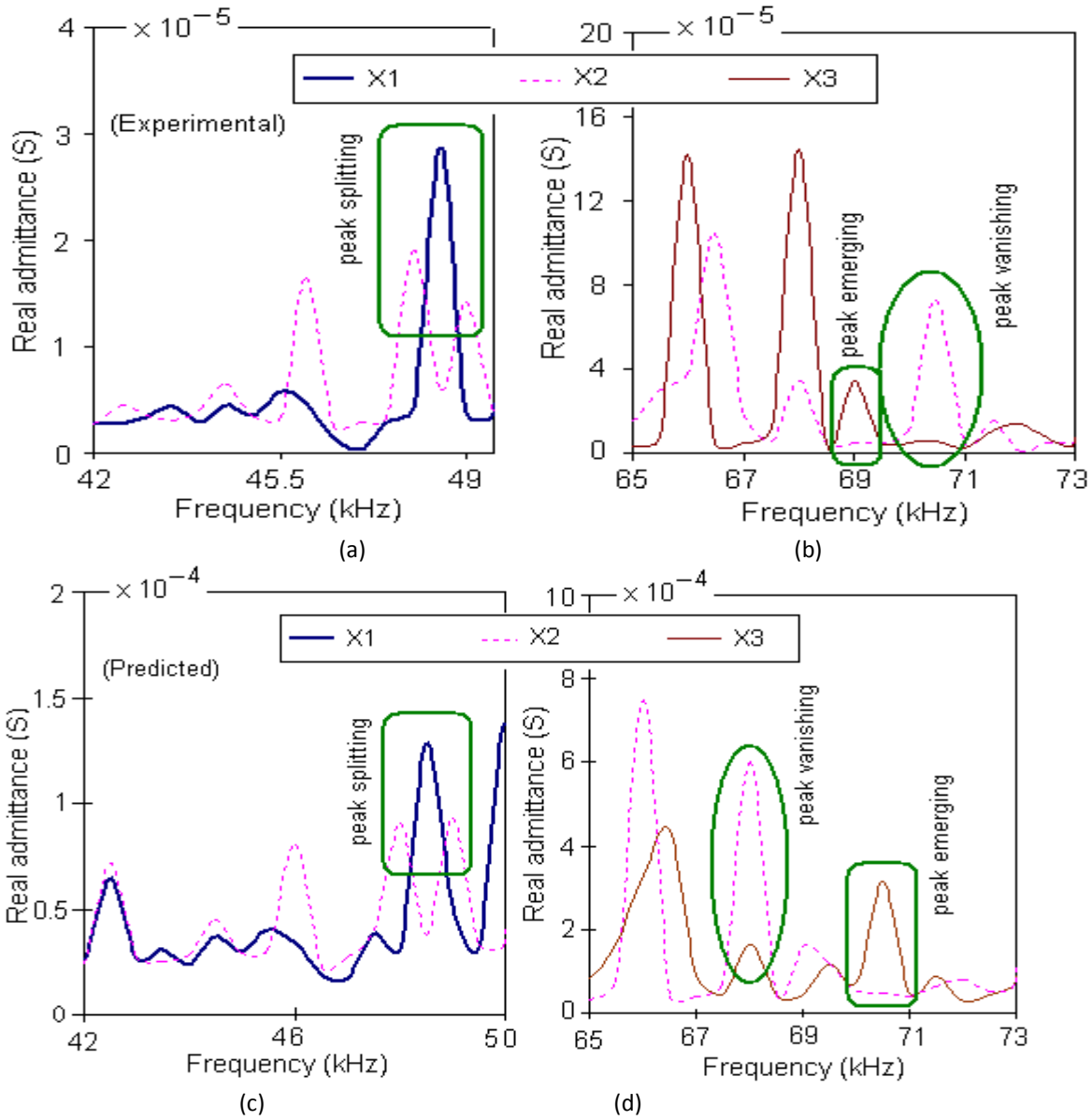

Fig. 8. Peak characterization versus damage propagation.
(a)Peak splitting in experimental signature (b) Peak emerging and vanishing in experimental signature
(c) Peak splitting in predicted signature (d) Peak emerging and vanishing in predicted signature

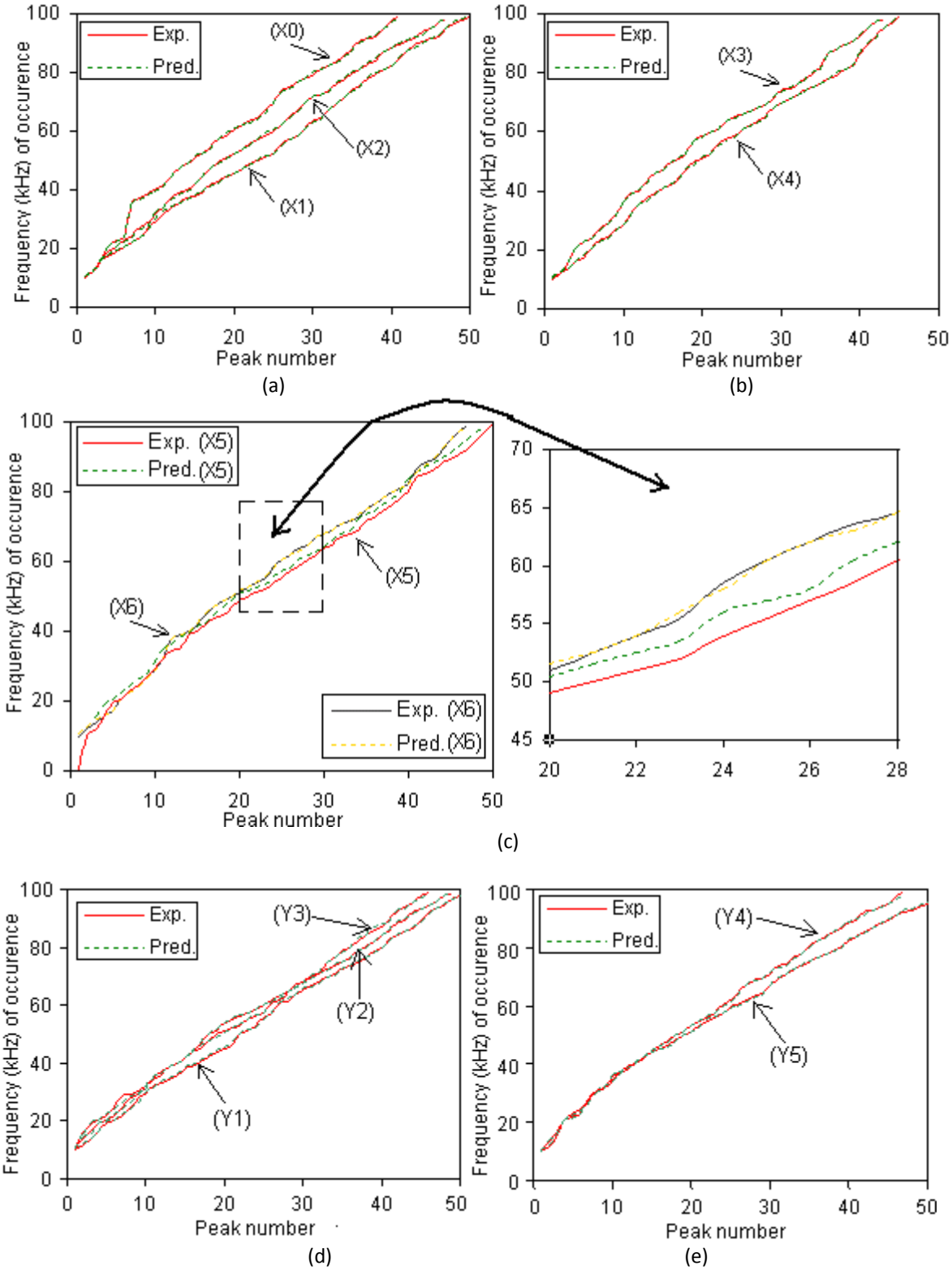

Fig.9. Comparison of experimental and predicted frequency of occurrence and number of peaks for various damaged cases

(a) X0, X1 and X2 (b) X3 and X4 (c) X5 and X6

(d) Y1 Y2 and Y3 (e) Y4 and Y5

Figure 9 shows the plots of peak number and its respective location on the frequency spectrum. The dotted line represents predicted frequency locations as against normal line, which represents experimental locations. Figure 9(a) shows the comparison of predicted and experimental real signatures for baseline X0, damaged states X1 and X2. Similarly Figures 9(b) and 9(c) compares admittance signatures of pairs of X3, X4 and X5, X6 respectively. Table 5 lists the comparison of experimental and predicted signatures for damage states along Y direction for plate Y. There exists satisfactory matching of predicted and experimental results for both plates, i.e the predicted matched well with the experimental frequency location (also see Figures 9 d-e).

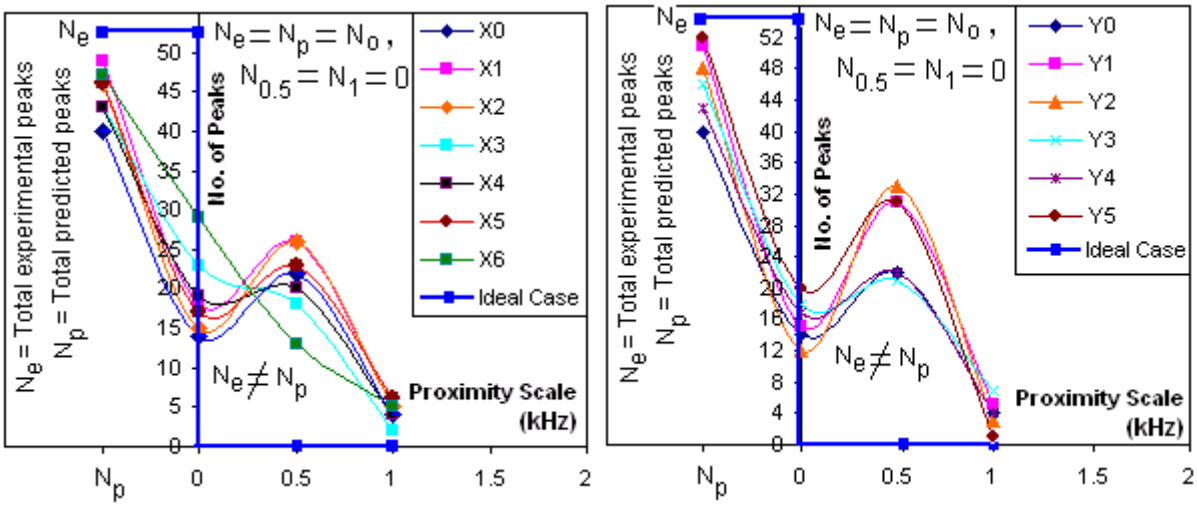

Fig.10. Proximity scale vs. number of peaks for various damage cases
(a) Plate X (b) Plate Y

However, the present study had measured the satisfactory proximity level of 3D predicted model using FPI scale as shown in Figure 10. For the considered range of 0-100 kHz there were peaks of over 50 in both experimental and predicted signatures. Predicted peak locations had shown significant proximity with experimental peak locations. The proximity of experimental and predicted peak locations is in between 0- 1.5 kHz. Let N_e represent number of experimental peaks, N_p be number of predicted peaks, N_0, $N_{0.5}$ and N_1 be peaks at 'frequency difference' of 0, 0.5 and 1 kHz respectively. 'Frequency difference' is the difference between predicted and experimental peak locations (Table 3). For higher frequency excitation models it is hard to have perfect match of both experimental and predicted signatures, however for low frequencies the match could be established (Yang et al 2005). Hence FPI has relevance only for high frequency excitation based PZT structure interaction model.

Table 5
Peak frequency comparison of experimental and predicted admittance signatures for plate Y

Y1		Y2		Y3		Y4		Y5	
E	P	E	P	E	P	E	P	E	P
10.0	10.5	10.0	10.5	10.0	10.5	10.0	10.5	10.5	10.0
12.0	12.5	16.5	16.0	14.0	14.5	12.0	12.5	13.5	14.0
14.0	14.0	19.0	19.5	17.0	16.0	15.5	16.0	16.5	16.0
16.5	16.5	20.5	20.5	19.0	19.0	20.5	20.5	20.5	20.5
19.0	19.5	22.0	22.5	20.5	20.5	22.0	21.5	23.0	22.5
20.5	20.5	24.5	24.0	22.0	22.5	23.0	23.0	24.5	24.0
22.0	22.5	28.5	26.5	24.5	24.0	28.0	26.5	27.0	26.5
24.5	24.0	29.0	28.5	28.0	26.5	30.5	31.0	30.5	30.0
28.0	26.5	30.5	30.0	29.0	29.0	32.0	32.5	32.0	32.0
29.0	29.5	32.0	31.0	32.0	32.0	34.5	34.0	36.0	36.5
32.0	31.5	34.5	35.0	34.5	35.5	37.0	36.5	37.0	37.5
33.0	33.5	36.0	36.5	37.0	36.5	38.0	38.5	39.0	38.5
34.5	35.0	39.0	38.5	39.0	38.5	40.5	41.0	40.0	40.0
36.0	36.5	40.0	40.0	40.0	40.0	42.5	42.5	42.0	42.5
38.0	38.5	42.0	42.0	42.0	42.0	44.0	44.5	44.0	44.0
39.0	39.5	44.0	44.5	44.0	44.0	46.5	46.5	45.0	45.0
40.5	41.0	45.0	46.0	46.5	47.0	48.0	47.5	46.5	46.0
42.0	42.5	47.5	48.0	50.0	50.0	49.5	49.5	48.0	47.5
44.0	44.5	50.0	49.0	51.0	51.5	51.0	51.0	50.0	50.0
45.0	45.5	51.0	50.5	54.0	54.0	53.0	53.0	51.0	51.0
46.5	47.5	52.0	52.0	55.0	55.5	55.0	55.0	53.0	52.5
50.0	50.0	53.0	53.5	56.0	56.5	56.0	56.5	55.0	55.5
51.0	51.5	55.0	55.0	57.5	57.5	57.5	57.5	56.0	56.5
53.0	52.5	56.0	56.5	58.5	58.5	60.5	60.0	57.5	57.5
55.5	55.0	57.5	57.5	60.0	60.0	62.0	61.5	59.5	59.0
57.5	57.5	60.5	61.5	62.0	61.5	64.5	63.5	60.5	60.0
60.5	61.5	62.0	62.5	63.5	63.5	67.0	67.0	62.0	61.5
61.0	62.5	64.5	64.5	64.5	64.5	68.5	68.5	63.0	62.5
63.5	63.5	67.0	66.5	67.0	66.0	69.5	69.5	64.5	63.5
65.0	65.5	68.0	67.5	68.0	67.5	71.0	71.5	67.0	67.0
67.0	66.5	69.5	69.0	69.5	70.0	73.5	73.0	69.5	70.0
68.0	67.5	71.5	71.0	71.0	71.5	74.5	74.0	71.0	71.0
69.5	69.5	72.5	72.0	74.5	75.0	76.5	76.0	72.0	72.5
71.0	70.5	73.5	74.0	76.5	76.5	77.5	77.5	73.5	74.0
72.5	72.5	74.5	75.0	78.5	78.0	80.5	80.0	75.0	75.5
73.5	73.5	76.5	76.0	80.0	80.0	82.0	82.0	76.5	76.5
74.5	75.5	78.5	78.5	82.0	83.0	84.0	83.0	77.5	77.5
76.5	76.5	80.5	80.0	84.0	84.0	85.5	85.5	78.5	78.5
78.5	78.0	82.0	82.0	86.0	87.0	86.5	87.0	80.5	80.0
80.0	79.5	84.5	84.0	87.0	88.0	88.5	89.0	82.0	82.5
82.5	82.0	85.5	860	89.5	89.0	89.5	90.0	84.0	84.0
84.0	84.0	88.0	88.5	92.0	92.5	92.0	91.0	85.5	85.0
85.5	85.5	89.5	90.0	94.0	93.5	93.0	93.0	86.5	86.5
86.5	87.0	92.0	91.5	95.5	95.5	94.0	94.0	88.5	88.5
89.5	89.0	93.0	93.5	97.5	97.0	95.0	95.0	89.5	90.0
92.0	91.5	94.5	94.5	99	98.5	97.5	96.5	91.0	91.0
93.0	93.0	95.5	95.5			99.0.	98.0	92.0	92.5
94.5	95.0	97.5	98.0					93.0	93.5
96.5	96.5	98.5	99.0					94.0	94.5
97.5	98.0							95.0	95.5
99.0	99.0							97.5	97.5
								98.5	98.5

Figure 10(a) shows peak numbers matched at proximity of 0 to 1 kHz and total number of predicted peaks versus experimental peaks for plate X. The ideal predicted model would have peaks predicted equal to that of experimental model. Moreover matching would be at proximity of 0 kHz, i.e $N_{0.5}$ = N_1 = 0. Figure 10(b) shows similar observation but for plate Y. However, if we consider the frequency difference less than 1 kHz as minor (negligible), the total number of peaks match was more or less equal to experimental peaks. In-fact, the 3D model had almost predicted all peaks of experimental signatures very satisfactorily. Thus we can say that signatures yielded by the 3D PZT-structure based predicted model had shown reasonable proximity with the experimental signatures. Additionally, this present study used FPI and RMSD to evaluate the 3D model for its successful implementation for damage analysis of plates.

4. Conclusions

In this paper, the application of 3D EMI model for damage assessment in plates was presented. A new frequency proximity index was proposed to study the proximity of 3D predicted model with experimental PZT-structure model. For this study, two types of damages were made along X and Y directions on two identical but unsymmetrical plates X and Y respectively. The experimental results were compared by a series of 3D predicted model based numerical simulations using finite element analysis. It was observed that the range of 0-100 kHz had more proximity between experimental and predicted signatures. The RMSD increased as the severity in damage increased in both plates for experimental and predicted results. In this paper the FPI and RMSD were used as complementary to each other successfully. i.e., the damages in both experimental and predicted study were quantified by RMSD index and the proximity of the results was compared by FPI scale. The trends of RMSD index and FPI scales have shown that the predicted model is promising for implementation into practical applications. Thus, this paper presented the application of 3D model to damage assessment of plates with introduction of FPI. and the paper is expected to be very useful for non destructive evaluation based SHM.

Acknowledgements

The authors would like to acknowledge Annamdas Krishna Preetham and Liu Hui for their assistance in experimental study.

References

Agilent Technologies, 2007. Test and measurement catalogue, California, U.S.A

Annamdas, V.G.M., Soh, C.K., 2010. Application of Electromechanical Impedance Technique for Engineering Structures: Review and Future Issues. Journal of Intelligent material systems and structures, 21(1): 41-59.

Annamdas, V.G.M., Soh, C.K., 2008. Three Dimensional Electromechanical Impedance Model for Multiple Piezoceramic Transducers with Structure Interaction Model. Journal of Aerospace Engineering, ASCE, 21(1), 35-44.

Annamdas, V.G.M., Soh, C.K., 2007a. Three Dimensional Electromechanical Impedance model I: Formulation of Directional Sum Impedance. Journal of Aerospace Engineering. ASCE. 20(1), 53-62.

Annamdas, V.G.M., Soh, C.K., 2007b. Three Dimensional Electromechanical Impedance model II: Damage analysis and PZT characterization. Journal of Aerospace Engineering. ASCE. 20(1), 63-71.

Annamdas V.G.M., Yang Y., 2012. Practical implementation of Piezo-ceramic sensors in monitoring of excavation for transit station construction in Singapore. Structural Control Health Monitoring, 19(2), 231 - 245.

Annamdas V.G.M., 2012. Facts of Piezo Impedance Technique in Crack Propagation Studies for a Engineering Structure. International Journal of Aerospace Sciences, 1(2), 8-15.

Annamdas, V.G.M., Yang Y., Soh, C.K., 2007. Influence of loading on the electromechanical admittance of piezoceramic transducers. Smart Materials and Structures, 16(5), 1888-1897.

ANSYS Inc., 2000. ANSYS Reference Manual, Release 5.6, Canonsburg, PA, USA.

Ayres, J.W., Lalande, F., Chaudhry, Z., Rogers, C.A., 1998. Qualitative impedance-based health monitoring of civil infrastructures. Smart Materials and Structures. 7(5), 599-605.

Chaudhry, Z., Joseph, T., Sun, F., Rogers, C., 1995. Local-area health monitoring of aircraft via piezoelectric actuator/sensor patches. Proceedings of SPIE North American Conference on Smart Structures and Materials, San Diego. CA. 26 Feb–3 March, 2443, 268–276.

Ghoshal, A., Harrison, J., Sundaresan, M.J., Hughes, D., Schulz, M.J., 2001. Damage detection testing on a helicopter flexbeam. Journal of Intelligent Material Systems and Structures. 12(5), 315-329.

Giurgiutiu, V., Zagrai, A.N., Bao, J., 2001. Piezoelectric wafer embedded active sensors for aging aircraft. Structural Health Monitoring, 1(1), 41-61.

Hewlett Packard., 1996. HP LF 4192A impedance analyzer Operation manual. Japan.

Hu, Y.H., Yang, Y.W., 2007. Wave propagation modeling of PZT sensing region for structural health monitoring. Smart Materials and Structures, 16(3), 706-716.

Liang, C., Sun, F.P., Rogers, C.A., 1996. Electro-mechanical impedance modelling of active material systems. Smart Materials and Structures, 5,171-186.

Park, G., Cudney, H., Inman, D.J., 2001. Feasibility of using impedance-based damage assessment for pipeline systems. Earthquake Engineering and Structural Dynamics, 30 (10), 1463–1474.

Park, G., Sohn, H., Farrar, C.R., Inman, D.J., 2003. Overview of piezoelectric impedance based health monitoring and path forward, The Shock and Vibration Digest, 35(6), 451-463.

Park, S., Yun, C.B., Roh, Y., Lee, J.J., 2005. Health monitoring of steel structures using impedance of thickness modes at PZT patches. Smart Structures and Systems, 1, 339–53.

PI Ceramic, 2007. Product Information Catalogue, Lindenstrabe, Germany, http://www.piceramic.de.

RS Components, 2007. Product Information Catalogue, Northants, UK, http://www.rs-components.com.

Sun, F.P., Chaudry, Z., Rogers, C.A., Majmundar, M., Liang, C., 1995. Automated real-time structure health monitoring via signature pattern recognition, Proceedings of the SPIE Conference on smart materials and structures, Feb. 27- Mar. 1, San Diego, California, 2443, 236-47.

Xu, J.F., Yang, Y.W., Soh, C.K., 2004. EM impedance-based structural health monitoring with evolutionary programming. Journal of Aerospace Engineering, ASCE, 17(4), 182-193.

Yang, Y.W., Annamdas, V.G.M., Wang, C., Zhou, Y., 2008. Application of multiplexed FBG and PZT impedance sensors for health monitoring of rocks. Sensors, 8(1), 271-289.

Yang, Y.W., Xu, J.F., Soh, C.K., 2005. Generic impedance-based model for structure-piezoceramic interacting system. Journal of Aerospace Engineering, ASCE, 18(2), 93-101.

Zhou, S.W., Liang, C., Rogers, C.A. 1996. An impedance-based system modeling approach for induced strain actuator-driven structures. Journal of Vibrations and Acoustics, ASME, 118(3), 323-331.